

## Longitudinal optical trapping and manipulating Rayleigh particles by spatial nonuniform coherence engineering

Jiayi Yu,<sup>1</sup> Ying Xu,<sup>1</sup> Shuqin Lin,<sup>1</sup> Xinlei Zhu,<sup>1,2</sup> Greg Gbur<sup>3,\*</sup> and Yangjian Cai<sup>1,2,†</sup>

<sup>1</sup>Shandong Provincial Engineering and Technical Center of Light Manipulations and Shandong Provincial Key Laboratory of Optics and Photonic Devices, School of Physics and Electronics, Shandong Normal University, Jinan 250014, China

<sup>2</sup>School of Physical Science and Technology, Soochow University, Suzhou 215006, China

<sup>3</sup>Department of Physics and Optical Science, University of North Carolina at Charlotte, Charlotte, North Carolina 28223, USA



(Received 23 May 2022; accepted 26 August 2022; published 19 September 2022)

Focused structured light fields with spatially nonuniform correlation can exhibit multiple focal points in the longitudinal direction, which suggests that they are suitable for longitudinal optical trapping. Due to the controllable nature of the longitudinal intensity distribution, this class of structured light fields not only can trap two high-index particles simultaneously, but also can manipulate them in the longitudinal direction.

DOI: [10.1103/PhysRevA.106.033511](https://doi.org/10.1103/PhysRevA.106.033511)

### I. INTRODUCTION

One half of the Nobel Prize in Physics 2018 was awarded to Ashkin “for the optical tweezers and their application to biological systems.” He performed the first demonstration of the capture and manipulation of particles using the radiation pressure of multiple laser beams in [1], and in [2] showed with collaborators that it is possible to trap dielectric particles using the radiation force from a single laser beam, a technique known as optical tweezing. Optical traps and tweezers have been extensively studied over the past half century since these seminal works, and they have become a powerful tool for the control and manipulation of a variety of small objects, such as viruses, biological cells, neutral atoms, DNA molecules, and dielectric particles [2–9]. While the principles of optical traps are well understood, refinements of the technique are still being actively investigated, including the use of structured light fields [10–13]. In this paper a different optical micromanipulation approach is demonstrated using the characteristics of a structured partially coherent light field.

Broadly speaking, a light field with a prescribed nontrivial amplitude, phase, and polarization distribution is called a structured light field. A Bessel beam is an example of a beam with a structured amplitude distribution, which makes it nondiffracting over extended propagation ranges; these beams have been used to trap and manipulate particles in multiple axial sites [14] and transport submicron particles over a distance of hundreds of micrometers [15]. Optical vortex beams are examples of beams with a structured phase that have been applied in a range of applications, such as twisting metal to create chirality in metal nanostructures [16]. Radially polarized beams have structured polarization, and a focused radially polarized double-ring-shaped beam has been used to trap two types of particles with different refractive indices

[17]. There are many other examples of using structured light for trapping and micromanipulation [18–20].

In the study of structured light, spatial coherence has emerged as a fourth intrinsic property of light fields that can be optimized for particular tasks. Light beams with reduced spatial coherence, referred to as partially coherent beams (PCBs), have been shown to perform better in some applications when compared to their coherent counterparts [21]. Optical trapping is a leading application of structured light and it is reasonable to believe that PCBs can play an important role in trapping, as their propagation and focusing characteristics can be controlled by the manipulation of spatial coherence. Auñón and Nieto-Vesperinas established a theory of the averaged optical force exerted by PCBs on a dipolar particle [22] and demonstrated that the simplest type of PCBs, Gaussian Schell-model beams, can produce exactly the same optical forces as a fully coherent laser beam [23].

Applications of partial coherence have been historically limited by the difficulty of designing tailored PCBs. However, Gori and Santarsiero proposed a new method for designing a wide variety of novel PCBs with prescribed correlation structures [24]. It has also been shown that the focused intensity distribution of a PCB can be affected dramatically by its correlation structure in the source plane [25]. Because the radiation forces of a light beam are directly related to the focused intensity, the radiation forces of a PCB can therefore be manipulated by tailoring the correlation structure, and it is a natural progression to investigate the trapping effect of PCBs with prescribed correlation structures. Over the past decade, researchers have conducted notable research along these lines. It has been shown that novel optical tweezers can be designed, for instance, that trap two types of Rayleigh particles simultaneously and modulate the trapping area [17,26–28].

Although the aforementioned results have achieved some novel trapping properties, they are restricted to the transverse focal plane. These earlier investigations were limited by the use of beams with a uniform correlation structure, such as Gaussian Schell-model beams, leaving many possible states

\*ggbur@unc.edu

†yangjiancai@suda.edu.cn

of spatial coherence unexplored. A distinct and broad class of beams includes those with a spatially variant correlation function, i.e., a nonuniformly correlated structure. The use of nonuniformly correlated structures extends the control of beams to include longitudinal effects as well as transverse, which makes it possible to trap and manipulate particles longitudinally by adjusting the coherence of light beams.

In this work we show the application of nonuniform coherence engineering in optical tweezing to realize the longitudinal trapping and control of particles. These results help fill the current gap in coherence modulation research, which only manipulates particles in the transverse focal plane.

## II. THEORETICAL MODELING

When incident light is scattered by a microparticle, an optical radiation force is produced by the exchange of momentum between the photon and the microparticle. We assume that the radius of the microparticle is much smaller than the wavelength of the incident light, in which case the microparticle can be treated as a simple point dipole and the Rayleigh scattering model is applicable [29]. Based on this model, the total radiation force acting on the dipole consists of two contributions: the scattering force and the gradient force. The former is proportional to the light intensity and is along the direction of light propagation, which is given by

$$\vec{F}_{\text{scat}} = \frac{\vec{e}_z n_a \alpha I}{c}, \quad (1)$$

where  $I$  is the intensity of the light illuminating the particle;  $\vec{e}_z$  is a unit vector along the beam propagation;  $c$  is the speed of light in a vacuum; and  $\alpha$  denotes the scattering cross section of the Rayleigh particle  $\alpha = \frac{8}{3} \pi k^4 R^6 [(\gamma^2 - 1)/(\gamma^2 + 2)]^2$ , with  $k$  the wave number,  $R$  the radius of the particle, and  $\gamma = n_p/n_a$ , with  $n_a$  and  $n_p$  the refractive index of the ambient medium and the particle, respectively. For a beam of finite size, there is also a transverse scattering component, but near the beam axis this component will be small and we therefore do not include it.

The gradient force is proportional to the gradient of the square of the electric field and can be expressed as

$$\vec{F}_{\text{grad}} = 2\pi n_a R^3 \left( \frac{\gamma^2 - 1}{\gamma^2 + 2} \right) \vec{\nabla} I / c. \quad (2)$$

The gradient force is directed along the gradient of light intensity and includes transverse and longitudinal components, i.e.,  $F_{\text{grad } x(y)}$  and  $F_{\text{grad } z}$ . The latter component is parallel or antiparallel to the scattering force and therefore the longitudinal gradient force must be larger than the scattering force in order to trap particles stably within the Rayleigh approximation.

From the expressions of the scattering force and gradient force, we can see that both of them are dependent upon the intensity distribution of the incident light. As noted above, a change of the spatial correlation properties of the light beam can therefore induce a change of the radiation force, as structured light with unusual correlations can exhibit novel intensity patterns [21]. In particular, structured light fields with nonuniform correlations can exhibit propagation features that are unachievable with uniform correlations. Such light fields have a self-focusing property [30] and we have analyzed

and verified this self-focusing [31]. Thus, structured light beams with nonuniform correlation are the perfect candidates to achieve longitudinal trapping and manipulation.

Next we discuss the unique advantages of structured light beams with nonuniform correlation in particle trapping and manipulation. A number of nonuniformly correlated beams have been studied in the past, such as a basic type of nonuniformly correlated beams and so-called Hermite nonuniformly correlated beams, and their propagation characteristics are well known [30,32]. In order to show that this nonuniformly correlated class of beams universally has unique advantages, we introduce another generalized set of higher-order two-dimensional sources in this paper.

We assume that we have a statistically stationary random scalar source. The second-order correlation properties of this light field can be described using the cross-spectral density (CSD) in the space-frequency domain. The CSD of the field at the source plane is defined as a two-point correlation function  $W(\mathbf{r}_1, \mathbf{r}_2) = \langle E^*(\mathbf{r}_1)E(\mathbf{r}_2) \rangle$ . Here  $E(\mathbf{r})$  denotes a component of the electric-field vector, the angular brackets indicate the ensemble average, and the asterisk denotes the complex conjugate. For brevity, we will work at a single frequency and omit the dependence on angular frequency in our expressions. To be a mathematically genuine correlation function, the CSD must correspond to a non-negative definite kernel, which can be given as a superposition integral as [24]

$$W(\mathbf{r}_1, \mathbf{r}_2) = \int p(\mathbf{v}) H^*(\mathbf{r}_1, \mathbf{v}) H(\mathbf{r}_2, \mathbf{v}) d^2\mathbf{v}, \quad (3)$$

where  $H(\mathbf{r}, \mathbf{v})$  is an arbitrary kernel and  $p(\mathbf{v})$  is a non-negative weight function, with  $\mathbf{v} = (v_x, v_y)$  a two-dimensional vector in Fourier space. In order to generate sources with a longitudinal manipulation capability and self-focusing extraordinary feature, we consider a kernel with a quadratic phase factor as

$$H(\mathbf{r}, \mathbf{v}) = \tau(\mathbf{r}) \exp[-ik(v_x + v_y)r^2], \quad (4)$$

where  $\tau(\mathbf{r}) = \exp(-r^2/4\omega_0^2)$  and  $\omega_0$  is the beam width. Then the weight function is set as a generalized higher-order form

$$p(\mathbf{v}) = \left( \frac{\beta^{m+1}}{\pi m!} \right) \mathbf{v}^{2m} \exp(-\beta \mathbf{v}^2), \quad (5)$$

where  $\beta$  is a positive real constant and  $m$  is the mode order. Then, according to Eq. (3), we obtain

$$W(\mathbf{r}_1, \mathbf{r}_2) = \exp\left(-\frac{r_1^2 + r_2^2}{4\omega_0^2}\right) \mu(\mathbf{r}_1, \mathbf{r}_2), \quad (6)$$

with the spectral degree of coherence given by

$$\mu(\mathbf{r}_1, \mathbf{r}_2) = \exp\left(-\frac{(r_1^2 - r_2^2)^2}{\delta^4}\right) L_m^0\left(\frac{(r_1^2 - r_2^2)^2}{\delta^4}\right). \quad (7)$$

Here  $\delta = \sqrt[3]{2\beta/k^2}$  is the spatial coherence length and  $L_m^0$  denotes the Laguerre polynomial of mode orders  $m$  and 0. We see that the above correlation function is an inhomogeneous function with Laguerre form. Therefore, we label this class of PCBs as Laguerre nonuniformly correlated (LNUC) beams. We infer from our earlier work [31] that such beams will also display self-focusing features and consequently also longitudinal manipulation capability; this is due to the fact that

the individual modes  $H(\mathbf{r}, \mathbf{v})$  of the beams possess a quadratic phase factor, which causes them to converge or diverge.

The propagation of a paraxial beam through an  $ABCD$  optical system can be handled by the extended Collins formula [33]

$$W(\boldsymbol{\rho}_1, \boldsymbol{\rho}_2) = \int W(\mathbf{r}_1, \mathbf{r}_2) G^*(\mathbf{r}_1, \boldsymbol{\rho}_1) G(\mathbf{r}_2, \boldsymbol{\rho}_2) d^2\mathbf{r}_1 d^2\mathbf{r}_2, \quad (8)$$

where  $G(\mathbf{r}, \boldsymbol{\rho}) = \frac{1}{i\lambda B} \exp(\frac{ikA}{2B}\mathbf{r}^2 - \frac{ik}{B}\mathbf{r} \cdot \boldsymbol{\rho} + \frac{ikD}{2B}\boldsymbol{\rho}^2)$  is the system propagator and  $\boldsymbol{\rho}_1$  and  $\boldsymbol{\rho}_2$  are the transverse spatial position vectors in the output plane. The quantities  $A$ ,  $B$ ,  $C$ , and  $D$  are the elements of a transfer matrix for the optical system. We insert the LNUC beam model into Eq. (8) and interchange the orders of the integrals to obtain

$$W(\boldsymbol{\rho}_1, \boldsymbol{\rho}_2) = \int p(\mathbf{v}) P(\boldsymbol{\rho}_1, \boldsymbol{\rho}_2, \mathbf{v}) d^2\mathbf{v}, \quad (9)$$

with

$$\begin{aligned} P(\boldsymbol{\rho}_1, \boldsymbol{\rho}_2, \mathbf{v}) \\ = \int H^*(\mathbf{r}_1, \mathbf{v}) H(\mathbf{r}_2, \mathbf{v}) G^*(\mathbf{r}_1, \boldsymbol{\rho}_1) G(\mathbf{r}_2, \boldsymbol{\rho}_2) d^2\mathbf{r}_1 d^2\mathbf{r}_2. \end{aligned} \quad (10)$$

We can analyze the intensity evolution of such beams by using the diagonal elements of the CSD, i.e.,  $S(\boldsymbol{\rho}) = W(\boldsymbol{\rho}, \boldsymbol{\rho})$ .

We now consider the case when a LNUC beam is focused by a thin lens of focal distance  $f$ . The transfer matrix of the system can be expressed as

$$\begin{pmatrix} A & B \\ C & D \end{pmatrix} = \begin{pmatrix} 1 & z+f \\ 0 & 1 \end{pmatrix} \begin{pmatrix} 1 & 0 \\ -\frac{1}{f} & 1 \end{pmatrix} = \begin{pmatrix} -\frac{z}{f} & z+f \\ -\frac{1}{f} & 1 \end{pmatrix}, \quad (11)$$

where  $z$  represents the axial distance from the focal plane to the output plane. Therefore,  $z < 0$ ,  $z > 0$ , and  $z = 0$  indicate that the output plane is located in front of, behind, and in the focal plane, respectively. In the following simulations, the focal distance of the thin lens is  $f = 1$  cm, while the power and the beam width of the incident LNUC beams are set as 50 mW and 1 cm, respectively. The coherence length and mode order are tunable parameters and will be given in each figure that follows.

### III. NUMERICAL RESULTS

Figure 1(a) shows isosurface plots of the propagation of focused LNUC beams for  $m = 1$  and  $\delta = 1$  cm. We clearly observe self-focusing and the positions of the minimum spot size, i.e., the real foci, appear in front of and behind the geometric focus ( $z = 0$ ). For convenience, the wavelength is taken to be that of common HeNe-type laser diodes,  $\lambda = 632.8$  nm; the results presented here are qualitatively similar for other wavelengths.

Figures 1(b) and 1(c) show how the on-axis intensity depends on the coherence length and mode order of focused LNUC beams on propagation. One clearly observes that there are two real foci which are displaced from the geometric focus. Furthermore, the initial beam parameters, coherence length, and mode order all affect the position of the real foci

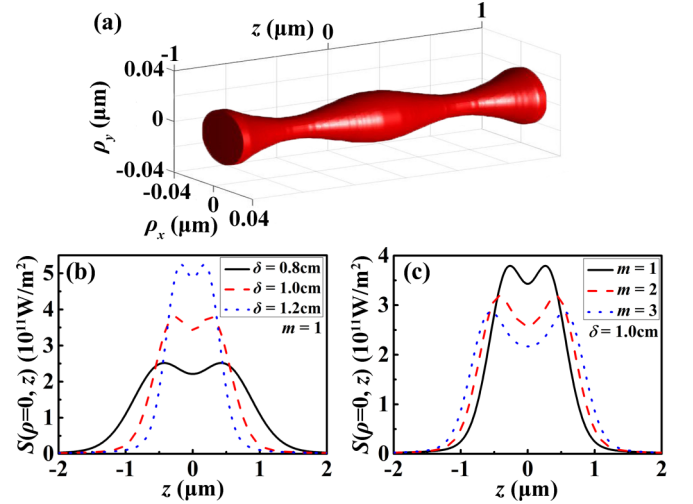


FIG. 1. (a) Isointensity plot and (b) and (c) on-axis intensity evolution of focused LNUC beams for different (b) coherence lengths and (c) mode orders.

and degree of focus. The positions of the real foci are further away from the geometric focus with decreasing coherence and increasing mode order, which means adjusting the initial beam parameters of the generated beams will manipulate the longitudinal intensity distribution, making it possible to achieve longitudinal particle trapping and manipulation.

We next consider the longitudinal gradient force on particles produced by focused LNUC beams. We choose two types of Rayleigh particles with refractive indices  $n_p = 1.59$  (i.e., glass spheres) and  $n_p = 1$  (i.e., air bubbles), with radii of  $R = 50$  nm. The ambient medium for both particles is water with refractive index  $n_a = 1.33$ . The other parameters are set the same as before.

Figure 2 shows the distributions of the scattering force  $F_{\text{scat } z}$ , longitudinal gradient force  $F_{\text{grad } z}$ , longitudinal

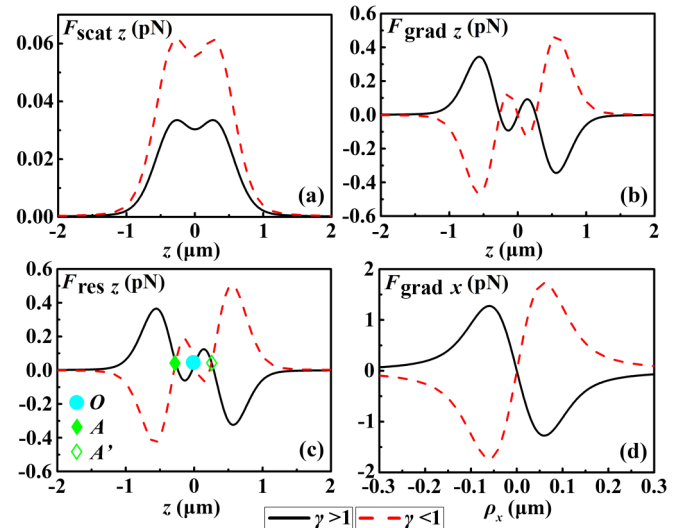


FIG. 2. Different radiant forces on two types of Rayleigh particles. The values  $\gamma > 1$  and  $\gamma < 1$  represent high- and low-index particles, respectively.

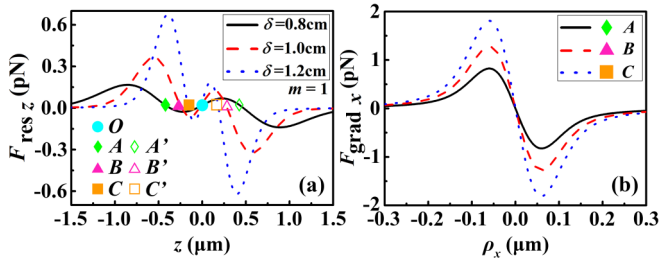


FIG. 3. (a) Longitudinal and (b) transverse gradient forces on the high-refractive-index Rayleigh particles for different states of spatial coherence.

resultant force  $F_{\text{res } z} = F_{\text{scat } z} + F_{\text{grad } z}$ , and transverse gradient force  $F_{\text{grad } x}$  of them acting on the high- ( $\gamma > 1$ ) and low- ( $\gamma < 1$ ) refractive-index Rayleigh particles by focused LNUC beams, with fixed initial beam parameters ( $m = 1$  and  $\delta = 1$  cm). From Fig. 2(a) we can see that the distribution of the scattering force of both Rayleigh particles is similar to the intensity distribution on propagation, as the scattering force is proportional to the intensity, as shown in Eq. (1).

We confirm from Fig. 2(b) that the values of the longitudinal gradient force can equal zero at several positions, which indicates that Rayleigh particles can be trapped around these zero points; however, such trapping depends on the relative value of the scattering force. Fortunately, comparing Figs. 2(a) and 2(b), we find the scattering force is negligible compared to the longitudinal gradient force.

The resultant of the longitudinal gradient force and scattering force is illustrated in Fig. 2(c), and we clearly find that there are multiple equilibrium points which could be used to trap particles. Furthermore, for a positive force, the direction of the longitudinal gradient force is along the  $+z$  direction and for a negative force it is along the  $-z$  direction. This means the low-refractive-index particles can be longitudinally trapped at the position  $O$  (i.e., geometric focus) and the high-refractive-index particles will be pushed from position  $O$  to positions  $A$  and  $A'$  and will eventually be longitudinally stable in such positions.

In order to demonstrate stable trapping in three dimensions, we must analyze the behavior of the radiation force in the transverse plane at the equilibrium points. As LNUC beams are circularly symmetric, we select the transverse gradient force in the  $x$  direction as representative of the general case. We find from Fig. 2(d) that, depending on the value of the radiant force, the transverse gradient force acting on the high-refractive-index Rayleigh particles pushes the particles inward (to optical axis). However, the transverse gradient force acting on the low-refractive-index Rayleigh particles pulls the particles outward (away from optical axis). Therefore, when the LNUC beams impinge on a collection of two types of particles, such beams will transversely disperse the low-refractive-index ones, screen out the high-refractive-index ones, and pull them out of the collection, stabilizing them at the equilibrium points away from the geometric focus.

Figure 3(a) shows how the longitudinal resultant radiation forces, acting on the high-refractive-index Rayleigh particles, depend on the coherence length. It is found that the positions of the equilibrium points, except for the geometric focus, are

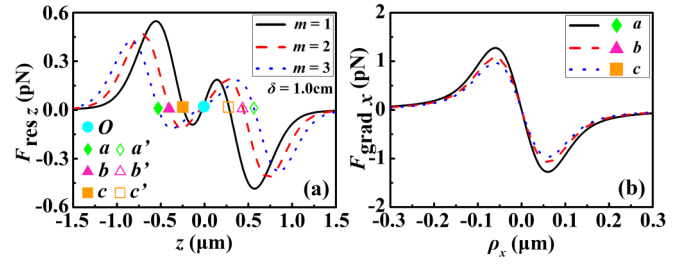


FIG. 4. (a) Longitudinal and (b) transverse gradient forces on the high-refractive-index Rayleigh particles for different mode orders.

related to the coherence of LNUC beams and the equilibrium points move away from the geometric focus as the coherence is decreased. This means that such beams can be used to trap the high-refractive-index Rayleigh particles first and then longitudinally move them away from or close to the geometric focus by adjusting the coherence of the incident beams. Since the coherence is continuously adjustable, the longitudinal position of the equilibrium points can be precisely manipulated. Furthermore, we find that the longitudinal trapping area for LNUC beams with low coherence is wider than that for the high coherence beam.

In addition, the amplitude of the radiation force decreases with decreasing coherence. This means that there is a trade-off between the position, range, and stability of trapping. Once the radiant force is reduced to a value that cannot overcome Brownian motion caused by the ambient thermal fluctuations, the particles can no longer be trapped stably. The comparison between the radiant force and Brownian force will be discussed in detail momentarily. Figure 3(b) shows the transverse gradient force acting on the high-refractive-index Rayleigh particles at stable equilibrium points ( $A$ ,  $B$ , and  $C$ ). We confirm from this result that the particles are pushed inward in the transverse plane, from which they can be stably trapped in the transverse plane. Therefore, combined with the conclusions from Fig. 3, it indicates that high-refractive-index Rayleigh particles can be stably trapped in the equilibrium points in three dimensions at locations other than the geometric focus.

The mode order is another important tunable parameter of LNUC beams that can be used to modulate the beam properties. Figure 4 shows the resultant radiation forces acting on high-refractive-index Rayleigh particles by focused LNUC beams with different mode order. The other parameters used are the same as those above. We confirm that the effect of increasing mode order is similar to that of decreasing the coherence of such beams. Increasing the LNUC mode order by one order, the equilibrium points will span a significant longitudinal distance, allowing for rough adjustment of position. Therefore, combined with fine-tuning of coherence, we can adjust the initial coherence length and mode order of such beams, making more flexible trapping and manipulation of particles.

We plot a detailed evolution of the position of the equilibrium point versus the coherence length for different mode orders in Fig. 5. The equilibrium points for trapping high-refractive-index particles will move away from the geometric focus as the coherence decreases and/or mode order increases. We find from this figure that the coherence can be

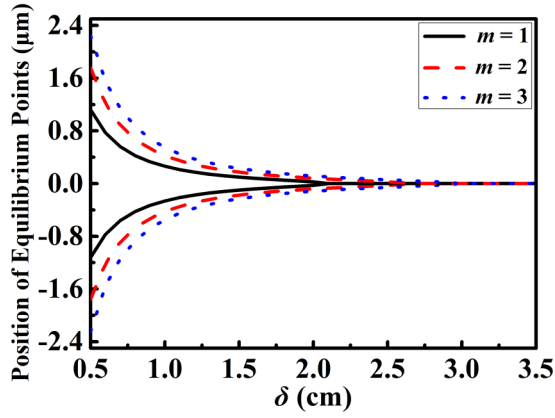


FIG. 5. Position of the equilibrium points versus the coherence length for different mode orders.

used for precision manipulation of the positions of the equilibrium points and the mode order can be used for rough manipulation. Therefore, users can determine for themselves which coherence length and mode order provide optimal results for their application from this figure.

Particles typically undergo Brownian motion due to thermal fluctuations of the ambient medium. Therefore, the Brownian force is another factor in the stability of optical traps. However, as long as the radiation force is appreciably larger than the Brownian force, the Brownian motion of the particles can be ignored. The magnitude of Brownian force can be obtained as  $|F_B| = (12\pi\kappa R\kappa_B T)^{1/2}$  according to the fluctuation-dissipation theorem of Einstein [34], where  $\kappa$  denotes the viscosity of the ambient medium ( $\kappa = 7.977 \times 10^{-4}$  Pa s for water at the temperature  $T = 300$  K) and  $\kappa_B$  denotes the Boltzmann constant. In our case, the radius of the particle  $R = 50$  nm and the Brownian force  $F_B = 2.5 \times 10^{-3}$  pN.

In Fig. 6 we compare the Brownian force with the various radiation forces as a function of coherence length, with mode order  $m = 1$ . In this figure,  $|F_{\text{grad } x}|_{\text{max}}$  represents the maximum transverse gradient force and  $|F_{\text{scat}}|_{\text{max}}$  represents the maximum longitudinal scattering force. Referring back to Fig. 4,  $|F_{\text{res } l-p}|_{\text{max}}$  and  $|F_{\text{res } l-v}|_{\text{max}}$  represent the maximum resultant forces at the large peak to the left of the geometric focus and the small valley to the left of the geometric focus, respectively, while  $|F_{\text{res } r-p}|_{\text{max}}$  and  $|F_{\text{res } r-v}|_{\text{max}}$  represent the

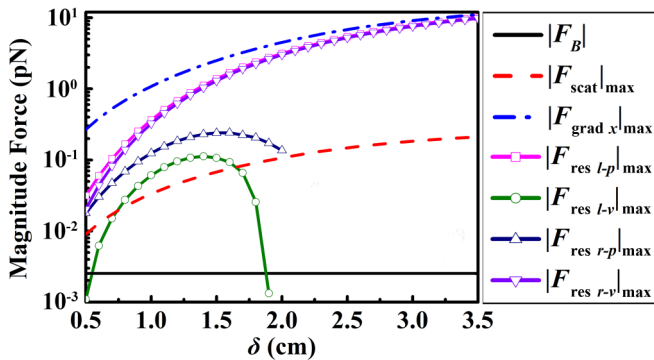


FIG. 6. Variations of Brownian force and radiation forces with coherent length with beam order  $m = 1$ .

maximum resultant forces at the small peak to the right of the geometric focus and the large valley to the right of the geometric focus, respectively.

It can be seen that the resultant forces are significantly larger than the Brownian force over a range of coherence values. When the coherence length of the beam is approximately 2 cm, the small peak and valley near the geometric focus disappear, removing the two longitudinal stable points near the ideal focus. It should be noted that even in such a case, and also the case when the coherence becomes lower than the critical value of 0.5 cm, the particles will still be coarsely trapped between the large left peak and large right valley in Fig. 4. This low coherence critical value is only for the initial beam power (50 mW) discussed in this paper. Therefore, users who use such structured light beams with low coherence for an application can increase the initial power of the incident beam as needed to overcome the Brownian motion.

#### IV. CONCLUSION

From the results shown above, we conclude that LNUC beams achieve longitudinal trapping and manipulation of Rayleigh particles. Furthermore, adjusting the coherence and mode order of LNUC beams allows fine and coarse control over the longitudinal position of particles.

It is worthwhile to say a few words about the physics that leads such beams to have their unusual trapping and manipulation properties. Equation (3) expresses the cross-spectral density as an integral over mutually incoherent modes of a beam. For the case of LNUC beams, as well as similar beams, Eq. (4) shows that each mode possesses a quadratic phase factor  $\exp[-ik(v_x + v_y)r^2]$ , which causes them to individually converge and diverge at different focal distances dictated by the values of  $v_x$  and  $v_y$ . Under the action of a focusing lens, these converging modes and diverging modes are focused on locations in front of and behind the geometric focus. The weighting function (5) determines which modes dominate and thus affects the position of the real foci. Therefore, adjusting the coherence (in effect, the shape of the weighting function) is a way to control which modes dominate in achieving longitudinally particle manipulation. It is worth noting that more complicated choices of weighting function may result in a more complex mode distribution, leading to even more sophisticated particle trapping and manipulation. In practice, these beams could be synthesized by using a pseudomode sampling superposition method [31,35], weighting them as different weight functions.

#### ACKNOWLEDGMENTS

This work was supported by the National Key Research and Development Program of China (Grant No. 2019YFA0705000), National Natural Science Foundation of China (Grants No. 12192254, No. 11974218, No. 12004218, and No. 91750201), Local Science and Technology Development Project of the Central Government (Grant No. YDZX20203700001766), China Postdoctoral Science Foundation (Grant No. 2020M680093), Shandong Provincial Natural Science Foundation of China (Grant No. ZR2020QA067), and Innovation Group of Jinan (Grant No. 2018GXRC010).

- [1] A. Ashkin, *Phys. Rev. Lett.* **24**, 156 (1970).
- [2] A. Ashkin, J. M. Dziedzic, J. E. Bjorkholm, and S. Chu, *Opt. Lett.* **11**, 288 (1986).
- [3] A. Ashkin and J. M. Dziedzic, *Science* **235**, 1517 (1987).
- [4] M.-C. Zhong, X.-B. Wei, J.-H. Zhou, Z.-Q. Wang, and Y.-M. Li, *Nat. Commun.* **4**, 1768 (2013).
- [5] A. D. Mehta, M. Rief, J. A. Spudich, D. A. Smith, and R. M. Simmons, *Science* **283**, 1689 (1999).
- [6] S. M. Block, L. S. B. Goldstein, and B. J. Schnapp, *Nature (London)* **348**, 348 (1990).
- [7] L. Oroszi, P. Galajda, H. Kirei, S. Bottka, and P. Ormos, *Phys. Rev. Lett.* **97**, 058301 (2006).
- [8] T. Kuga, Y. Torii, N. Shiokawa, T. Hirano, Y. Shimizu, and H. Sasada, *Phys. Rev. Lett.* **78**, 4713 (1997).
- [9] V. Garcés-Chávez, D. Roskey, M. D. Summers, H. Melville, D. McGloin, E. M. Wright, and K. Dholakia, *Appl. Phys. Lett.* **85**, 4001 (2004).
- [10] M. Woerdemann, *Structured Light Fields Applications in Optical Trapping, Manipulation, and Organisation* (Springer, Heidelberg, 2012).
- [11] A. Forbes, M. D. Oliveira, and M. R. Dennis, *Nat. Photonics* **15**, 253 (2021).
- [12] Y. Yang, Y. Ren, M. Chen, Y. Arita, and C. Rosales-Guzmán, *Adv. Photon.* **3**, 034001 (2021).
- [13] E. Otte and C. Denz, *Appl. Phys. Rev.* **7**, 041308 (2020).
- [14] V. Garcés-Chávez, D. McGloin, H. Melville, W. Sibbett, and K. Dholakia, *Nature (London)* **419**, 145 (2002).
- [15] T. Čižmár, V. Garcés-Chávez, K. Dholakia, and P. Zemánek, *Appl. Phys. Lett.* **86**, 174101 (2005).
- [16] K. Toyoda, K. Miyamoto, N. Aoki, R. Morita, and T. Omatsu, *Nano Lett.* **12**, 3645 (2012).
- [17] Y. Zhang, B. Ding, and T. Suyama, *Phys. Rev. A* **81**, 023831 (2010).
- [18] A. Ashkin and J. M. Dziedzic, *Appl. Phys. Lett.* **19**, 283 (1971).
- [19] C.-H. Chen, P.-T. Tai, and W.-F. Hsieh, *Appl. Opt.* **43**, 6001 (2004).
- [20] G. Gouesbet, *J. Quant. Spectrosc. Radiat. Transfer* **225**, 258 (2019).
- [21] Y. Cai, Y. Chen, J. Yu, X. Liu, and L. Liu, *Prog. Opt.* **62**, 157 (2017).
- [22] J. M. Auñón and M. Nieto-Vesperinas, *J. Opt. Soc. Am. A* **29**, 1389 (2012).
- [23] J. M. Auñón and M. Nieto-Vesperinas, *Opt. Lett.* **38**, 2869 (2013).
- [24] F. Gori and M. Santarsiero, *Opt. Lett.* **32**, 3531 (2007).
- [25] G. Gbur and T. D. Visser, *Opt. Lett.* **28**, 1627 (2003).
- [26] C. Zhao and Y. Cai, *Opt. Lett.* **36**, 2251 (2011).
- [27] Z. Liu and D. Zhao, *Opt. Express* **20**, 2895 (2012).
- [28] B. Yang, Y. Chen, F. Wang, and Y. Cai, *J. Quant. Spectrosc. Radiat. Transfer* **262**, 107518 (2021).
- [29] L. Novotny and B. Hecht, *Principles of Nano-Optics* (Cambridge University Press, Cambridge, 2012).
- [30] H. Lajunen and T. Saastamoinen, *Opt. Lett.* **36**, 4104 (2011).
- [31] S. Lin, J. Wu, Y. Xu, X. Zhu, G. Gbur, Y. Cai, and J. Yu, *Opt. Lett.* **47**, 305 (2022).
- [32] J. Yu, F. Wang, L. Liu, Y. Cai, and G. Gbur, *Opt. Express* **26**, 16333 (2018).
- [33] S. A. Collins, *J. Opt. Soc. Am.* **60**, 1168 (1970).
- [34] K. Okamoto and S. Kawata, *Phys. Rev. Lett.* **83**, 4534 (1999).
- [35] X. Zhu, J. Yu, Y. Chen, F. Wang, O. Korotkova, and Y. Cai, *Appl. Phys. Lett.* **117**, 121102 (2020).